# Femtosecond four-wave-mixing spectroscopy of interacting magnetoexcitons in semiconductor quantum wells

S. Yokojima,* T. Meier,† V. Chernyak, and S. Mukamel
*Department of Chemistry and Rochester Theory Center for Optical Science and Engineering, University of Rochester, Rochester, New York 14627*
(Received 17 August 1998)

Nonlinear exciton equations for one- and two-exciton variables, obtained by mapping the two-band model onto the molecular (Frenkel) Hamiltonian, are applied to calculate resonant optical nonlinearities in two-dimensional semiconductors in a strong perpendicular magnetic field. The polarization dependence of the time-resolved four-wave-mixing signals provides a direct probe for the two-exciton manifold as well as for the asymmetry of the particle-particle and particle-hole Coulomb interactions. [S0163-1829(99)01116-9]

## I. INTRODUCTION

The effective dimensionality of semiconductor nanostructures is changed in a strong magnetic field due to the confinement of the relative electron-hole motion in the directions perpendicular to the applied field. The effects of this confinement on the optical response have been studied extensively both experimentally[1–7] and theoretically.[4,8–12]

In this paper we calculate the time-domain-degenerate four-wave-mixing (FWM) signal emitted in the $2\mathbf{k}_2-\mathbf{k}_1$ direction from a semiconductor quantum well. FWM is a convenient tool in the study of exciton dynamics.[13–19] This background-free technique provides detailed information on the energies and oscillator strengths of one- and two-exciton states, as well as the magnitude of the coupling between them.[7] We investigate the signatures of bound biexcitons and exciton-exciton scattering in two-dimensional semiconductors in a strong perpendicular magnetic field. Interesting effects are studied which arise from the asymmetry between the particle-particle and particle-hole Coulomb interaction, and from the two-exciton manifold structure induced by the symmetry of the spin and real-space parts of the two-exciton wave functions.

It has been shown[20] that the asymmetry of the Coulomb interaction determines the magnitude of the exciton-exciton interactions in strong magnetic field which affects the thermodynamic properties of the exciton gas. We have shown that this asymmetry strongly affects the nonlinear optical response as well, since it is the only parameter that controls the biexciton state formation.[11]

In order to introduce the proper level of theory required for describing these effects, let us consider the exciton creation (annihilation) operators $B^\dagger(B)$ (a precise definition will be given in Sec. II). The lowest level of theory for the optical response based on the equations of motion for the Heisenberg operators incorporates only the $\langle B\rangle$ variables, and factorizes all higher-order quantities. The resulting equation is known as the semiconductor Bloch equation (SBE) in the case of semiconductors,[18] the time-dependent Hartree-Fock (TDHF) approximation[21] for conjugated molecules,[22,23] or the local-field approximation for molecular nanostructures.[17,24] The projection onto a single one-exciton state results in a nonlinear Landau-Ginzburg equation.[15,25]

Unbound two-exciton and bound biexciton states are not accounted for properly using this level of description. A higher level of theory is required which involves the two-exciton dynamical variables $\langle BB\rangle$ as well as the one-exciton $\langle B\rangle$ variables.[26] In the absence of dephasing processes, $\langle B\rangle$ and $\langle BB\rangle$ are the only variables that need to be considered to obtain exact expressions for the third-order optical response.[12,26] This theory avoids the explicit calculation of two-exciton states, relating the optical nonlinearities directly to the exciton-exciton scattering matrix.[27,28]

Effects of dephasing induced by the coupling to phonons have been incorporated for Frenkel exciton systems by using a closed system of equations of motion for $\langle B\rangle$ and $\langle B^\dagger B\rangle$ variables, the latter representing the exciton density matrix.[14,29] The same level of theory for semiconductor systems yields SBE's with dephasing,[18,30–32] which have been successfully applied for the interpretation of ultrafast nonlinear optical phenomena in semiconductors and semiconductor nanostructures. These equations have already been used to analyze the linear and nonlinear optical properties of magnetoexcitons in two[9] and three[10] dimensions. However, since two-exciton $\langle BB\rangle$ variables are not included as independent variables, the structure of two-exciton resonances is completely missed. Equations of motion that include the $\langle B\rangle$, $\langle BB\rangle$ and $\langle B^\dagger B\rangle$ variables and interpolate between the theories of Refs. 26 and 14 were developed subsequently.[17,29] Green-function expressions which represent the combined effects of exciton transport and two-exciton resonances have been developed and applied to various Frenkel exciton systems.[33–36] In the absence of vibronic coupling the method was extended to molecular aggregates made of three-level molecules,[37] and to semiconductors.[12,38] Finally, it has been shown that a complete description of third-order optical processes should be based on equation of motion for the $\langle B\rangle$, $\langle BB\rangle$, $\langle B^\dagger B\rangle$, and $\langle B^\dagger BB\rangle$ variables.[17,28] A recent derivation of these nonlinear exciton equations (NEE's) which includes a microscopic calculation of the phonon-induced relaxation kernels was presented in Ref. 39. Similar equations, based on the same many-body-induced hierachy of equations of motion, have been derived recently for Wannier exciton systems.[12,16,40–43] Compared to Frenkel excitons, numerical solutions of the NEE's applied to Wannier systems are con-

 

siderably more expensive. Therefore, these are typically performed in the coherent limit, where only single- and two-exciton amplitudes need to be considered.[16,43–45] Only a few calculations beyond the coherent limit using simplified models have been reported so far.[46,47]

Our primary interest in the present paper is to investigate the possible use of FWM techniques to probe the coherent dynamics which involves the two-exciton states. We therefore use simplified NEE's which include $\langle B\rangle$ and $\langle BB\rangle$ variables only, and neglect the effects of phonon-induced dephasing.

Recently, it has become evident that the polarization dependence of the FWM signals in semiconductor nanostructures can only be accounted for by including variables which go beyond the TDHF approximation.[16,40,41,44,48–59] For example, excitation-induced dephasing processes[48–51] have been attributed to exciton-exciton scattering.[16,40,44] The effects of bound biexcitons[52–58] and signatures of two-exciton states contributing in higher orders in the field ($\chi^{(5)}$) have been studied as well.[41,59] In order to account for the polarization dependence of the FWM signals, it is necessary to include the two-exciton variables $\langle BB\rangle$ with four different angular momenta [see Eqs. (2.8)–(2.13)].[11]

Green-function expressions for the third-order response of semiconductors derived by mapping the two-band model onto the Frenkel Hamiltonian[12] have recently been applied to calculate the frequency-domain two-color pump-probe signal from two-dimensional semiconductors in a strong perpendicular magnetic field.[11] In this paper we extend this study to the time-domain and predict the resonant femtosecond FWM signals for the same model. In Sec. II we combine the two-exciton basis set and matrix elements calculated in Ref. 11 with the NEE's (Ref. 12) to obtain equations of motion for one- and two-exciton variables of a two-dimensional semiconductor quantum well in a strong perpendicular magnetic field. These equations are applied in Sec. III to calculate the time-integrated and time-resolved FWM signals. The dependences on the polarization of exciting pulses and on the asymmetry of Coulomb interaction are carefully examined. Finally, our results are summarized in Sec. IV.

## II. NEE'S FOR MAGNETOEXCITONS

We start by introducing the two-band model Hamiltonian of semiconductors in real space,[11,12]

$$H=\sum_{m_1n_1} t^{(1)}_{m_1n_1}a^\dagger_{m_1}a_{n_1}+\sum_{m_2n_2} t^{(2)}_{m_2n_2}b^\dagger_{m_2}b_{n_2} +\tfrac{1}{2}\sum_{m_1n_1k_1l_1} V^{(1)}_{m_1n_1k_1l_1}a^\dagger_{m_1}a^\dagger_{n_1}a_{k_1}a_{l_1} +\tfrac{1}{2}\sum_{m_2n_2k_2l_2} V^{(2)}_{m_2n_2k_2l_2}b^\dagger_{m_2}b^\dagger_{n_2}b_{k_2}b_{l_2} +\tfrac{1}{2}\sum_{m_1n_2k_2l_1} W_{m_1n_2l_1k_2}a^\dagger_{m_1}b^\dagger_{n_2}b_{k_2}a_{l_1}. \quad (2.1)$$

Here $a_{n_1}$ ($a^\dagger_{n_1}$) and $b_{n_2}$ ($b^\dagger_{n_2}$) are the Fermi annihilation (creation) operators of electrons and holes, respectively, with the commutation relations

$$a_{n_1}a^\dagger_{m_1}+a^\dagger_{m_1}a_{n_1}=\delta_{m_1n_1},\qquad b_{n_2}b^\dagger_{m_2}+b^\dagger_{m_2}b_{n_2}=\delta_{m_2n_2}. \quad (2.2)$$

We adopt the following convention: Latin indices with a subscript 1 (2), e.g., $m_1$ ($m_2$) stand for electron (holes), including spin variables. Electron-hole pairs are denoted by Latin indices without subscripts $m\equiv(m_1m_2)$.

The total Hamiltonian of the system coupled to a driving electric field $\mathcal{E}(\mathbf{r},\tau)$ has the form

$$H_T(\tau)=H-\int d\mathbf{r}\,\mu(\mathbf{r})\mathcal{E}(\mathbf{r},\tau), \quad (2.3)$$

with the dipole operator

$$\mu(\mathbf{r})\equiv\sum_{m_1m_2}\mu_{m_1m_2}(\mathbf{r})(a^\dagger_{m_1}b^\dagger_{m_2}+b_{m_2}a_{m_1}). \quad (2.4)$$

Following Refs. 11 and 12, we introduce the electron-hole (exciton) operators

$$B^\dagger_{m_1m_2}\equiv a^\dagger_{m_1}b^\dagger_{m_2},\quad B_{m_1m_2}\equiv b_{m_2}a_{m_1}, \quad (2.5)$$

and expand the Hamiltonian [Eq. (2.1)] and the commutation relations for the exciton operators in powers of the normally ordered $B$ and $B^\dagger$ operators, retaining the terms which contribute to a given order. For the third-order response the commutation relations should be expanded up to second-order, whereas terms up to the fourth order should be retained in the Hamiltonian.[11,12] The Hamiltonian represented in terms of the exciton operators can be used to derive equations of motion for the $\langle B_m\rangle$ and $\langle B_mB_n\rangle$ variables by employing pure state factorization,[26] which neglects the phonon-induced dephasing and leads to the following closed nonlinear exciton equations for the one- and two-exciton variables[11,12,26,60]:

$$i\frac{d\langle B_n\rangle}{d\tau}=\sum_m h_{nm}\langle B_m\rangle-\mathcal{E}_n+\sum_{mpq}U_{nm,pq}\langle B^\dagger_m\rangle\langle B_pB_q\rangle+\sum_{mpq}P_{nm,pq}\langle B^\dagger_m\rangle(\langle B_p\rangle\mathcal{E}_q+\langle B_q\rangle\mathcal{E}_p), \quad (2.6)$$

$$i\frac{d\langle B_nB_{n'}\rangle}{d\tau}-\sum_{mm'}(h_{nm}\delta_{n'm'}+\delta_{nm}h_{n'm'})\langle B_mB_{m'}\rangle-\sum_{mm'}U_{nn',mm'}\langle B_mB_{m'}\rangle=-(\delta_{nm}\delta_{n'm'}-P_{nn',mm'})(\mathcal{E}_m\langle B_{m'}\rangle+\langle B_m\rangle\mathcal{E}_{m'}), \quad (2.7)$$

where $h$ is the one-exciton Hamiltonian acting in the one-exciton space whose eigenvalues give the one-exciton energies. The operators $U$ and $P$ act in the two-exciton space, and describe exciton-exciton Coulomb interactions and electron (hole) exchange, respectively,[11,12] and $\mathcal{E}_m$ is defined by $\mathcal{E}_m(\tau)\equiv\int d\mathbf{r}\,\mu_m(\mathbf{r})\mathcal{E}(\mathbf{r},\tau)$. Equations (2.6) and (2.7) are exact for the response up to third order, and are equivalent to the equations derived in Ref. 42. In the strong-magnetic-field limit, we can neglect the Coulomb-induced coupling between different Landau levels. Assuming that the electrons and holes belong to the first Landau level and taking spin into account, Eqs. (2.6) and (2.7) result in the following six equations:

$$i\hbar\frac{d\langle B_+\rangle}{d\tau}=\epsilon_0\langle B_+\rangle-\mathcal{E}_+ +\sum_{ni} r_n U_{n,i}\langle B_+^\dagger\rangle\langle BB_i\rangle+\sum_{nj} r_n U_{n,j}\langle B_-^\dagger\rangle\langle BB_j\rangle+\sum_{nl} r_n U_{n,l}\langle B_-^\dagger\rangle\langle BB_l\rangle+\frac{1}{\pi}\langle B_+^\dagger\rangle\langle B_+\rangle\mathcal{E}_+, \tag{2.8}$$

$$i\hbar\frac{d\langle B_-\rangle}{d\tau}=\epsilon_0\langle B_-\rangle-\mathcal{E}_- +\sum_{nj} r_n U_{n,j}\langle B_+^\dagger\rangle\langle BB_j\rangle+\sum_{nk} r_n U_{n,k}\langle B_-^\dagger\rangle\langle BB_k\rangle+\sum_{nl} r_n U_{n,l}\langle B_+^\dagger\rangle\langle BB_l\rangle+\frac{1}{\pi}\langle B_-^\dagger\rangle\langle B_-\rangle\mathcal{E}_-, \tag{2.9}$$

$$i\hbar\frac{d\langle BB_i\rangle}{d\tau}=\sum_{i'} H_{i,i'}\langle BB_{i'}\rangle-4r_i\mathcal{E}_+\langle B_+\rangle, \tag{2.10}$$

$$i\hbar\frac{d\langle BB_j\rangle}{d\tau}=\sum_{j'} H_{j,j'}\langle BB_{j'}\rangle-r_j\mathcal{E}_+\langle B_-\rangle-r_j\mathcal{E}_-\langle B_+\rangle, \tag{2.11}$$

$$i\hbar\frac{d\langle BB_k\rangle}{d\tau}=\sum_{k'} H_{k,k'}\langle BB_{k'}\rangle-4r_k\mathcal{E}_-\langle B_-\rangle, \tag{2.12}$$

$$i\hbar\frac{d\langle BB_l\rangle}{d\tau}=\sum_{l'} H_{l,l'}\langle BB_{l'}\rangle-r_l\mathcal{E}_+\langle B_-\rangle-r_l\mathcal{E}_-\langle B_+\rangle. \tag{2.13}$$

Here the subscript of the one-exciton variable $\langle B\rangle$ stands for the $z$ component of the angular momentum $J_z$ whereas the subscripts $i$, $j$, $k$, and $l$ of the two-exciton variable $\langle BB\rangle$ represent the two-exciton manifolds involved in the optical response. Here we use the same discrete basis set introduced in Ref. 11, which classifies the $\langle BB\rangle$ variables by their angular momentum $J$ and $J_z$. Following Refs. 11 and 55, we neglect the light holes and consider only the transitions between heavy holes ($J=\frac{3}{2}$, $J_z=\pm\frac{3}{2}$) and the conduction band ($J=\frac{1}{2}$). This gives rise to two degenerate single-exciton resonances that can be excited by circularly polarized light $\sigma^+$ and $\sigma^-$, respectively (Fig. 1). Since a two-exciton state consists of two electrons and two holes, its possible angular momenta are $J=2$, with $J_z=2$ (which is denoted by index $i$), $J_z=0$ ($j$), and $J_z=-2$ ($k$); and $J=1$, with $J_z=0$ ($l$),[11] as shown in Fig. 1. The real-space part of the two-exciton wave function is either symmetric ($J=1$, index $l$) or antisymmetric ($J=2$, indices $i$, $j$, and $k$) with respect to exchange of the two electrons and two holes (without spin exchange).[11] $r_m$ is given by $\langle\Psi_m|\Psi^{(2)}_{\mathbf{p}=\mathbf{0}}\rangle$, where $\Psi_m$ ($\Psi^{(2)}_{\mathbf{p}}$) are discrete (continuous) two-exciton basis sets defined in Ref. 11. $\epsilon_0$ is one-exciton energy (the small energy shift induced by the magnetic $B$ field has been neglected), and $H$ is the two-exciton Hamiltonian. $\mathcal{E}_\pm$ is given by $\mu\sigma_\mp\cdot\mathbf{E}$, where $\mathbf{E}$ is defined in Eq. (A1). The matrices $U$ and $H$ were given in Ref. 11 using a two-exciton discrete basis set.

We adopt the following form for the Coulomb potentials[11] with short-range asymmetry:

$$V_{eh}(\mathbf{r},\mathbf{r}')=-\frac{\alpha}{|\mathbf{r}-\mathbf{r}'|}\{1+\kappa_{eh}\exp[-|\mathbf{r}-\mathbf{r}'|^2/r_0^2]\}, \tag{2.14}$$

$$V_{ee}(\mathbf{r},\mathbf{r}')=V_{hh}(\mathbf{r},\mathbf{r}')=\frac{\alpha}{|\mathbf{r}-\mathbf{r}'|}\{1+\kappa_{ee}\exp[-|\mathbf{r}-\mathbf{r}'|^2/r_0^2]\}, \tag{2.15}$$

In all calculations the asymmetry-length parameter $r_0$ is chosen to be the same for all potentials, whereas the parameters $\kappa_{eh}$ and $\kappa_{ee}$ which represent its magnitude have been varied. This asymmetry strongly affects the nature of the two-exciton states represented by the $\langle BB\rangle$ variables.

The signatures of two-exciton dynamics in the time-integrated and time-resolved FWM signals of two-dimensional semiconductors in a strong perpendicular magnetic field will be explored next.

## III. FOUR-WAVE-MIXING SIGNALS FROM MAGNETOEXCITONS

We have calculated the FWM signal emitted in the direction $2\mathbf{k}_2-\mathbf{k}_1$ (this is known as the two-pulse self-diffraction geometry). By invoking the rotating-wave approximation [Eqs. (A2)–(A14)], we can recast Eqs. (2.8)–(2.13) in a form suitable for numerical calculations.

The exciting field is made of two pulses,

$$\mathbf{E}(t)=\sum_{j=1,2}\mathbf{E}_j(t)e^{i\mathbf{k}_j\cdot\mathbf{r}-i\omega_j t}+\mathbf{E}_j^*(t)e^{-i\mathbf{k}_j\cdot\mathbf{r}+i\omega_j t}, \tag{3.1}$$

where the pulse envelopes are given by

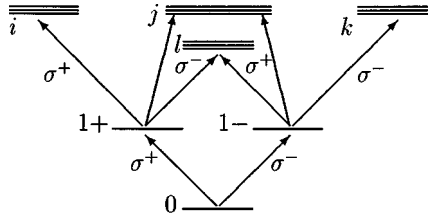


FIG. 1. Exciton level scheme for a GaAs quantum well. The two-exciton states are shown with indices $i$ ($J=2$, $J_z=2$), $j$ ($J=2$, $J_z=0$), $k$ ($J=2$, $J_z=-2$), and $l$ ($J=1$, $J_z=0$).

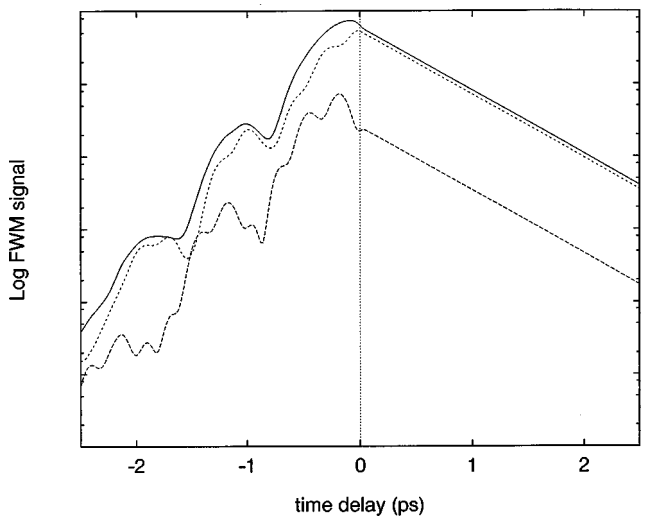


FIG. 2. Time-integrated FWM signal for $\kappa_{ee}=0$, $\kappa_{eh}=1$. Short dashed line: linearly copolarized pulses. Long dashed line: linearly cross-polarized pulses. Solid line: circularly copolarized pulses.

$$\mathbf{E}_1(t)=\mathbf{E}_1 e^{-[t/\bar{t}_1]^2}, \quad \mathbf{E}_2(t)=\mathbf{E}_2 e^{-[(t-T)/\bar{t}_2]^2}, \quad (3.2)$$

where $T$ is the time delay between pulses.

When the detection does not resolve the polarization orientation,[55] the time-integrated FWM signal $S_{INT}(T)$ is given by

$$S_{INT}(T)=\int dt|\mathbf{P}^{(-1|2)}(t,T)|^2. \quad (3.3)$$

Here $\mathbf{P}^{(-1|2)}(t,T)$ is the polarization in the $2\mathbf{k}_2-\mathbf{k}_1$ direction, as defined in Appendix A. Our numerical calculations will focus on the case $\kappa_{eh}>\kappa_{ee}$, where bound biexciton states are formed, giving rise to distinct signatures in FWM.[52–58] The symmetry of the two-dimensional magnetoexcitons in the strong-magnetic-field limit allows us to use a simple procedure to calculate the two-exciton states.[11]

Pulse durations are $\bar{t}_1=\bar{t}_2=30$ fs. The phenomenological dephasing times (see Appendix A) are taken as $\hbar/\gamma_1=2\hbar/\gamma_2=1$ ps. We use the GaAs parameters $m_e=0.0665$, $m_h=0.457$, and $\epsilon_0=13.74$. We set $\omega_1=\omega_2=-11.5$ meV, which corresponds to the one-exciton energy for $H=10$ T. (The zero of the energy scale corresponds to the one-exciton energy in the absence of a magnetic field.) The asymmetry length is taken as $r_0=4$ in units of the characteristic magnetic length $l_H=\sqrt{\hbar/eH}=8.1$ nm. The two-exciton basis set was truncated at $N_0=100$, which is sufficient to describe the two-exciton states fairly well.[11] The equations of motion were integrated using a fourth-order Runge-Kutta algorithm with a time step of 0.5 fs. $S_{INT}$ for $\kappa_{ee}=0$ and $\kappa_{eh}=1$ is given in Fig. 2 for three configurations of the polarization of the incoming fields: (A) Linearly copolarized pulses $\mathbf{E}_1=\mathbf{E}_2=(1,0)$; both $\mathbf{E}_1$ and $\mathbf{E}_2$ are linearly polarized in the $x$-direction (short dashed line). (B) Linearly cross-polarized pulses $\mathbf{E}_1=(1,0)$, $\mathbf{E}_2=(0,1)$; $\mathbf{E}_1(\mathbf{E}_2)$ is linearly polarized along the $x(y)$ direction (long dashed line). (C) Circularly copolarized pulses $\mathbf{E}_1=\mathbf{E}_2=(1/\sqrt{2},i/\sqrt{2})$; both $\mathbf{E}_1$ and $\mathbf{E}_2$ have $\sigma_+$ polarizations (solid line).

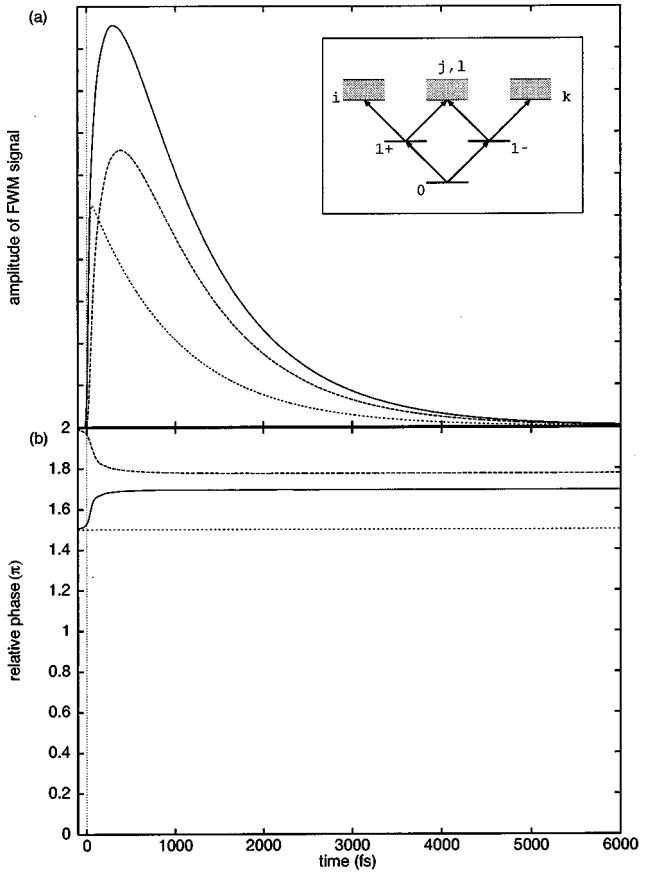


FIG. 3. Time-resolved amplitude (a) and phase (b) of the FWM signal for time delay $T=0$ fs, linearly copolarized pulses, and symmetric Coulomb potential. $\kappa_{ee}=0$ and $\kappa_{eh}=0$. Solid line: the total amplitude of the FWM signal. Long dashed line: the amplitude of the Coulomb scattering component of the FWM signal. Short dashed line: the amplitude of the Pauli blocking component of the FWM signal. The inset shows the level scheme corresponding to Fig. 1. The patched part shows the two-exciton continuum.

For positive time delays the signals decrease monotonically, whereas an oscillatory behavior is observed for negative delays.[16] This is also expected from the frequency-domain calculation of $\chi^{(3)}$ for zero magnetic field.[41] In both long and short dashed lines the duration of the two maxima (or minima) are about 250 fs, which corresponds to the lowest bound biexciton state. (The biexciton binding energies for the lowest and second lowest bound biexcitons are 16.5 and 4.0 meV, respectively.) The solid line in Fig. 2 shows the oscillation with about 1ps, since it only couples to the antisymmetric wave function. (Symmetric and antisymmetric wave functions refer to the symmetry of the real-space part of the two-exciton wave function.) The largest binding energy of the antisymmetric wave function is 4.0 meV, which corresponds to a period of about 1 ps. This feature is different from previously investigated quantum-well systems, where no bound biexcitons were excited for co-circularly polarized excitation.[16,59] Bound excitons exist in our case due to the combined action of the magnetic field together with the asymmetry of the Coulomb interaction, and are excited for this polarization configuration. The calculated relative strength of the time-integrated FWM signal for three different polarizations is in good qualitative agreement with

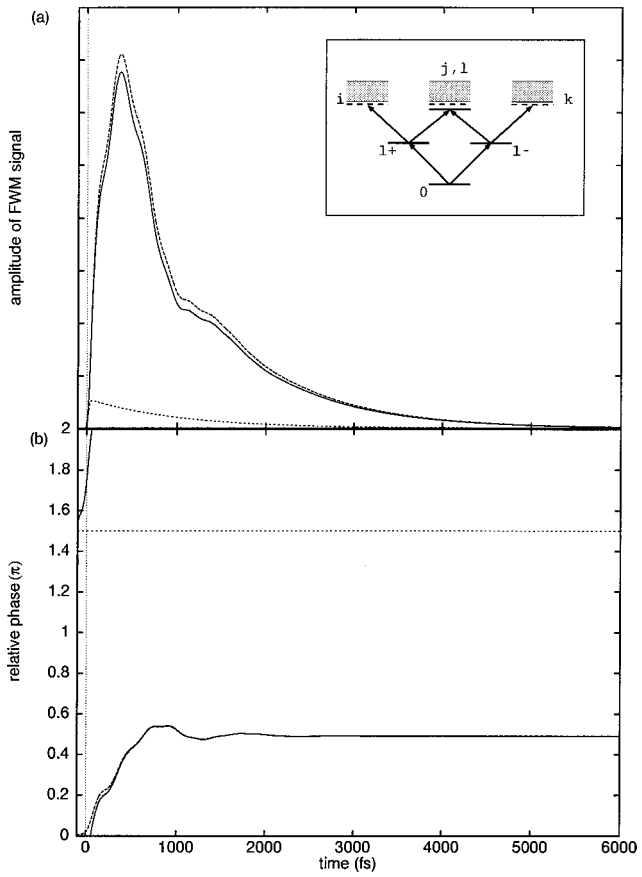


FIG. 4. The same as Fig. 3 but for asymmetric calculation potential $\kappa_{ee}=0$ and $\kappa_{eh}=1$. The inset shows the level scheme. The symmetric and antisymmetric bound biexciton levels are indicated by the solid and dashed lines below the two-exciton continuum, respectively.

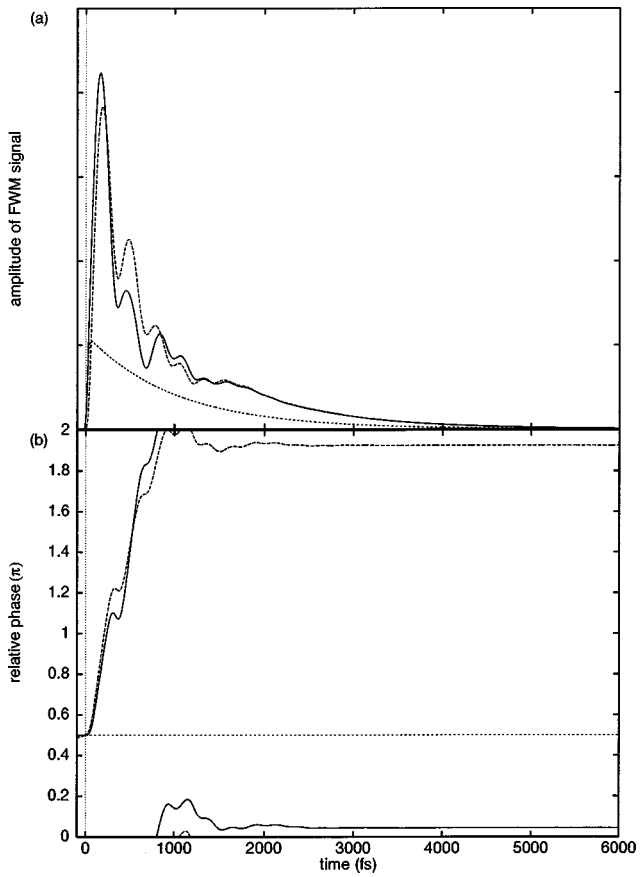


FIG. 5. Same as Fig. 3, but for linearly cross-polarized pulses.

zero magnetic-field experiments.[16,59]

The heterodyne detected time-resolved FWM signal is given by

$$S(t;T)=\mathbf{P}_x^{(-1|2)}(t,T). \tag{3.4}$$

Here $\mathbf{P}_x$ denotes the $x$ component of the complex two-dimensional polarization vector $\mathbf{P}$ (see the discussion below). These signals are displayed in Figs. 3–9. In all figures, the upper panel (a) shows the amplitude of FWM signal $|\mathbf{P}(t)|$, and the lower panel (b) shows the relative phase $\Delta\phi(t)$ with respect to the exciting pulse $\mathbf{E}_1(t)$. $\Delta\phi(t)$ is defined as follows.

For (A) and (B) polarizations, the $y$ component of the polarization in $2\mathbf{k}_2-\mathbf{k}_1$ is zero, and $\Delta\phi$ can be simply defined as

$$\Delta\phi(t)=\omega_1 t-\phi_x(t), \tag{3.5}$$

where $\phi_x(t)$ is the phase of the $x$-component of the FWM signal. For the (C) polarization, the $2\mathbf{k}_2-\mathbf{k}_1$ signal is $\sigma_+$ polarized, and the $x$ and $y$ components of the FWM signal have the same relative phase with respect to the exciting pulse $\mathbf{E}_1(t)$. We can thus again use Eq. (3.5) as the definition of $\Delta\phi$.

The FWM signal consists of two contributions: Pauli blocking (phase-space filling) and the exciton-biexciton transitions induced by the Coulomb interaction. In Eqs. (A11) and (A12) the former nonlinearity is proportional to $E\langle B^\dagger\rangle\langle B\rangle$, whereas the latter is proportional to $\langle B^\dagger\rangle\langle BB\rangle$. These contributions are given by the short dashed and long dashed lines, respectively, and the total signal is given by solid line. The phase of the Pauli blocking term is time independent in time-resolved FWM with resonant excitation.[22,23] This is because we select a single one-exciton level for each spin, which gives only one Pauli blocking term in Eqs. (A11) and (A12). This can also be seen analytically in the short-pulse limit. Setting $\epsilon_0=\omega_1=\omega_2$, the Pauli blocking term in Eqs. (B1) and (B2) does not have any time-dependent phase factor.

During the short-time period when the optical field is applied, the Pauli blocking term is dominant. We can see that the phase of the FWM signal (solid line) starts from the same value as the phase of the Pauli blocking term (short dashed line) in Figs. 3–9.

We have investigated three cases: symmetric Coulomb interaction $\kappa_{ee}=0$ and $\kappa_{eh}=0$ (Fig. 3), medium asymmetry $\kappa_{ee}=0$ and $\kappa_{eh}=1$ (Figs. 4–6), and strong asymmetry $\kappa_{ee}=0$ and $\kappa_{eh}=2$ (Figs. 7–9). The relevant level schemes were shown in the inset of Ref. 11. The manifold of levels obtained here (Fig. 1 or the inset of Figs. 3, 4, and 7) is more general than the commonly used level scheme for FWM in GaAs quantum wells,[55,57,58,61] since it includes antisymmetric two-exciton levels with total angular momentum $J=2$.

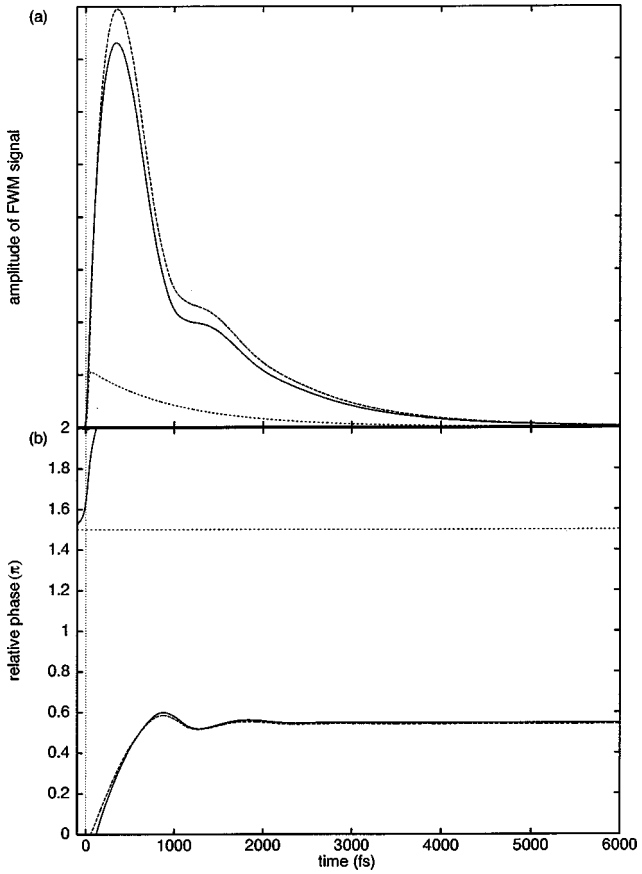


FIG. 6. Same as Fig. 4, but for circularly copolarized pulses.

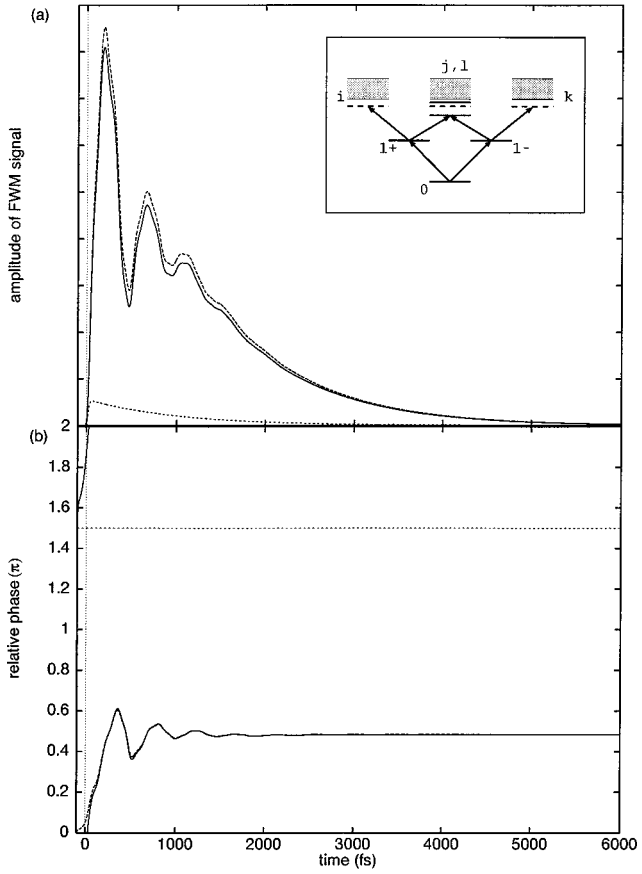


FIG. 7. Same as Fig. 4, but for strong Coulomb asymmetries $\kappa_{ee}=0$ and $\kappa_{eh}=2$.

These show interesting signatures in FWM signals of magnetoexcitons in a strong magnetic field.

All three signals displayed in the upper panel of Fig. 3 have a single maximum. The time of the maximum of the amplitude of the Pauli blocking term (short dashed line) is determined by the duration of the exciting field. Subsequently, this term undergoes free-induction decay. The amplitude of the Coulomb scattering term (long dashed line) reaches its maximum at later times, determined by the dephasing time scale.

This long rise time has been interpreted using a nonlinear Ginzburg-Landau-like wave equation for the $1s$ exciton amplitude.[15,25] That analysis is based on a two-level system with a local-field-like nonlinearity arising from factorization of the higher correlations. This has been shown to correspond to the local-field approximation (LFA).[17,24] The LFA which is equivalent to the TDHF approximation can be extended in various ways. One possibility is to introduce population variables $\langle B^{\dagger}B\rangle$.[13] Since we do not incorporate pure dephasing, population variables can be factorized as $\langle B^{\dagger}\rangle\langle B\rangle$, and do not appear in the equation of motion. However, two-exciton variables play a similar role on the shape and the amplitude of the FWM signal. In the third-order equations of motion, the Coulomb interaction term couples either $\langle B^{\dagger}\rangle\langle BB\rangle$ or $\langle B^{\dagger}B\rangle\langle B\rangle$ depending on the approximation scheme. In both cases, we can regard these terms as sources for the third-order response for a weak electric field (in our case, without pure dephasing the nonlinear response can be expressed using the two-exciton variables $\langle BB\rangle$, whereas the population terms $\langle B^{\dagger}B\rangle$ can be factorized exactly). Since these sources are long living, i.e., they decrease slowly with the dephasing time and not with the short duration of the exciting fields, the integration of these sources in the equation of motion gives a maximum of the signal at a delayed time. Here the effect of the Coulomb-interaction terms and the Pauli blocking term on the amplitude of the FWM signal are comparable. Since we excite single excitons resonantly, the amplitude of the FWM signal induced by the Pauli blocking term (which does not depend on Coulomb interaction) is not affected by changing the parameters $\kappa_{ee}$ and $\kappa_{eh}$. Thus the FWM signals from the Pauli blocking terms in Figs. 3, 4, and 7 have the same magnitude. The amplitude of FWM signal in Fig. 3 is small compared to Figs. 4 and 7. This is consistent with the fact that we do not have a nonlinear optical signal for symmetric Coulomb interaction.[11] The small signal coming from Coulomb interaction is an artifact of our truncated two-exciton basis set, as discussed in Ref. 11.

As shown in Appendix B, the phase of the Coulomb term starts from 0 ($2\pi$) for the linearly copolarized pulses.[23] It then varies smoothly with time, converging to a value which is close to $2\pi$. Inspection of Eqs. (B6) and (B7) shows that the small change of the phase indicates that the two-exciton levels contributing to $\langle B_{\pm}\rangle^{(-1|2)}_{Coulomb}(0,t)$ are mainly located near twice the one-exciton energy.

For $\kappa_{ee}=0$ and $\kappa_{eh}=1$, we have calculated the amplitude and relative phase of the FWM signal for our three polarization configurations: (A) linearly copolarized pulses (Fig. 4),

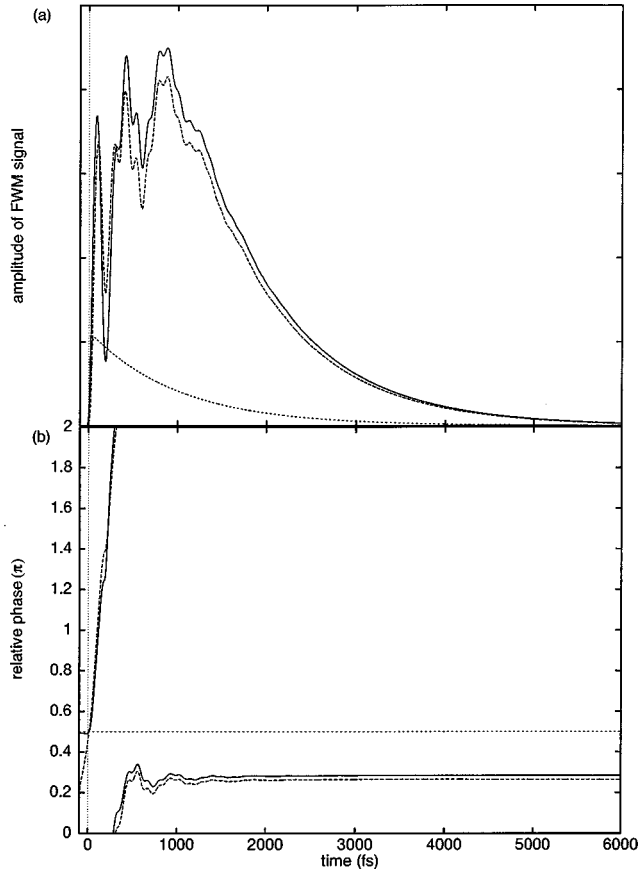


FIG. 8. Same as Fig. 7, but for linearly cross-polarized pulses.

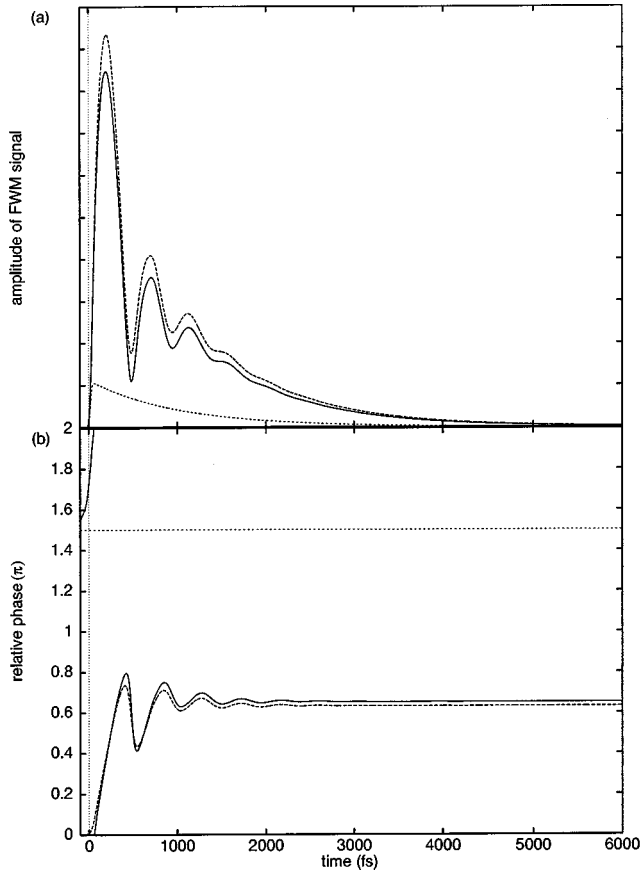


FIG. 9. Same as Fig. 7, but for circularly copolarized pulses.

(B) linearly cross-polarized pulses (Fig. 5), and (C) circularly copolarized pulses (Fig. 6). Our system has one symmetric and three antisymmetric bound biexciton levels. These correspond to the lowest symmetric and antisymmetric states.[11] The symmetric and antisymmetric bound biexciton levels are indicated by the solid and dashed lines just below the patched part (two-exciton continuum) of the inset of Fig. 4. In all three cases, the FWM signal shows quantum beats. However, their pattern is different. The signal in Fig. 6 resembles that of Fig. 3, but with one additional feature. The oscillation period is about 1 ps, which corresponds to the binding energy of the lowest antisymmetric state (4.0 meV). Circularly copolarized pulses excite only the $\langle BB_i\rangle$ variables and do not show beats corresponding to the symmetric states.

Figure 4 is similar to Fig. 6. It is hard to trace the origin of the oscillations in Fig. 4. The oscillations in Fig. 5 come from the lowest symmetric biexciton level. It has a binding energy of 16.5 meV which corresponds to a period of about 250 fs. The origin of the difference of the amplitude of FWM signal between linearly copolarized and linearly cross-polarized FWM signal may be attributed to the cancellation of the different paths shown in the inset. The signal in Fig. 5 is much weaker than that in Fig. 4. This can be easily seen by comparing the Pauli blocking terms in Figs. 4 and 5, noting the fact that the amplitudes of the FWM signal from the Pauli blocking term in Figs. 4 and 5 are the same as discussed for the Pauli blocking terms in Figs. 3, 4, and 7.

To clarify this point, let us examine Eq. (B1). Since $\vec{\sigma}_-\cdot\mathbf{E}_2\vec{\sigma}_+\cdot\mathbf{E}_1^*$ and $\vec{\sigma}_+\cdot\mathbf{E}_2\vec{\sigma}_-\cdot\mathbf{E}_1^*$ have the same sign for linearly copolarized pulses, the contributions of the three Coulomb scattering terms $K_{i_1}$, $K_{j_1}$, and $K_{l_1}$ to the FWM signal have the same sign as well, whereas for linearly cross-polarized pulses $\vec{\sigma}_-\cdot\mathbf{E}_2\vec{\sigma}_+\cdot\mathbf{E}_1^*$ and $\vec{\sigma}_+\cdot\mathbf{E}_2\vec{\sigma}_-\cdot\mathbf{E}_1^*$ have an opposite sign. Thus the terms $K_{j_1}$ and $K_{i_1}$ cancel each other. Since $K_{i_1}$ has a factor 2, it also cancels the continuum part of $K_{l_1}$. As a result, the lowest symmetric level in $K_{l_1}$ and the lowest antisymmetric level in $K_{i_1}$ (with a factor $\frac{1}{2}$) contribute to the FWM signal with opposite signs. Because of these large cancellations for linear cross-polarized excitation, we can clearly see the oscillations originating from the lowest symmetric level compared to the linear copolarized pulses, where the oscillation is buried in the signal of the lowest antisymmetric level and the continuum.

The relative phase also carries interesting information in Figs. 4–6. Because of the different polarization of the exciting pulses, the relative phase of the Pauli blocking term in linearly copolarized pulses (Fig. 4) and in circularly copolarized pulses (Fig. 6) is $3\pi/2$, whereas in linearly cross-polarized pulses it is $\pi/2$. The phase of the Coulomb scattering term starts from 0 and converges to about $\pi/2$ for linear and circularly copolarized pulses. These results are reproduced analytically for short pulses by taking limits for $t$ (Appendix B). The terms $f_n/(\Delta_n+i\gamma_2)$ $(n=i_1,j_1,l_1)$ in Eq. (B7) have a bound biexciton part and a continuum part. The two have opposite phases resulting in a $\pi/2$ phase for large $t$. The Coulomb scattering term for linearly cross-polarized pulses (Fig. 5) shows a different phase near $t=0$ compared to Figs. 4 and 6. This is because of the small contribution from the first-order term in $t$ in Eq. (B6): $2\Sigma_{i_1}f_{i_1}-\Sigma_{j_1}f_{j_1}$

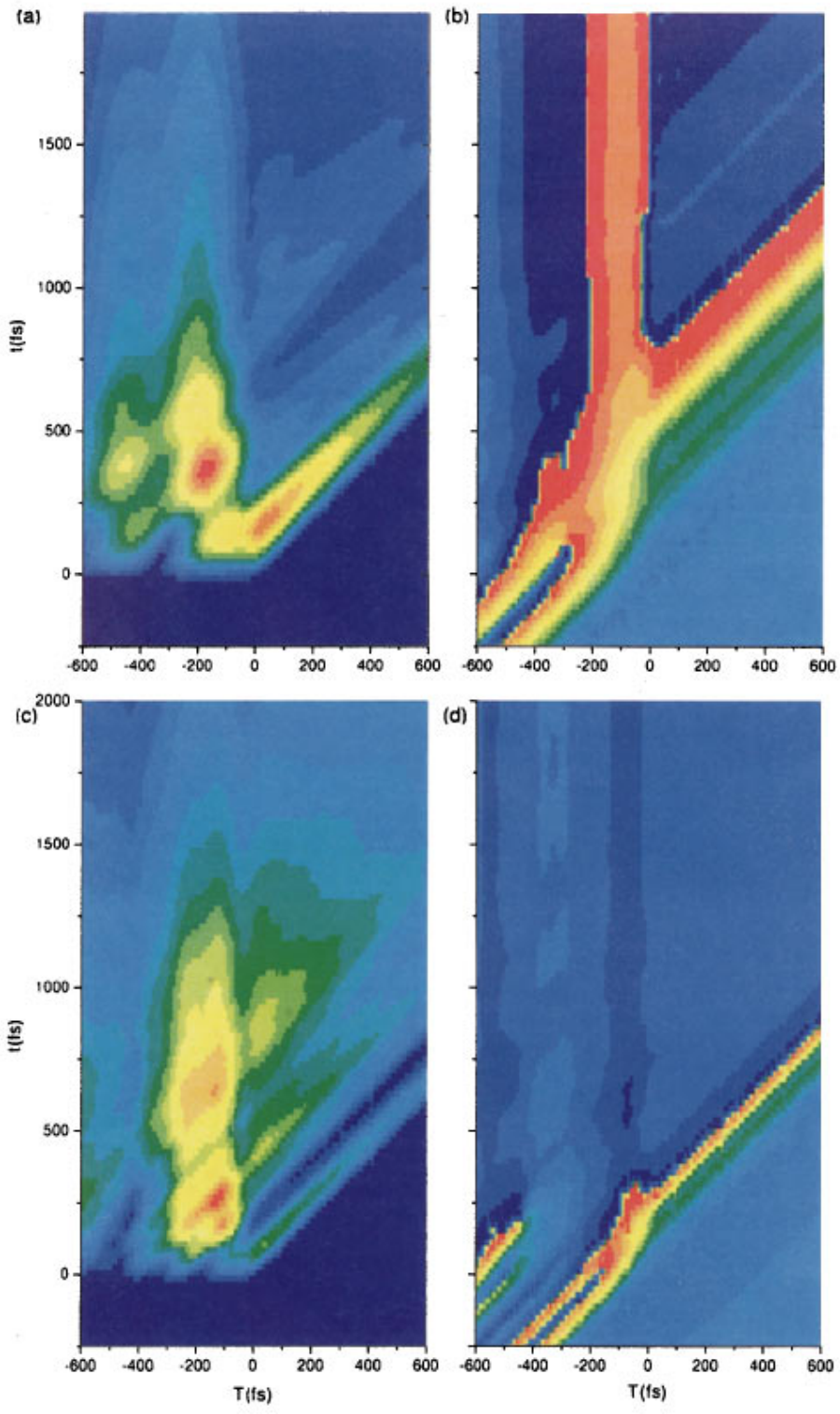


FIG. 10. (Color) Time-resolved amplitude [(a) and (c)] and phase [(b) and (d)] of FWM signal. (a) and (b) $\kappa_{ee}=0$ and $\kappa_{eh}=1$. (c) and (d) $\kappa_{ee}=0$ and $\kappa_{eh}=2$. Magnitude of the amplitude and phase (from 0 to $2\pi$) are shown by the 16 levels of color. *X* axis: delay time *T*. *Y* axis: real time *t*. Linearly cross-polarized pulses. [Large, red (corresponding to 100–93.75 % of the maximum value); yellow, green, and blue, small (0–6.25%).]

$-\Sigma_{l_1} f_{l_1} \simeq 0$. The phase of the Coulomb scattering term is $\pi/2$, because we have a factor *i* in the second order term in Eq. (B6). A small difference between Eq. (B6) and our numerical results comes from the finite (30 fs) pulse duration. The large change of the phase of the Coulomb scattering term with increasing time *t* is also related to the cancellation. Because of the different sign between $\vec{\sigma}_- \cdot \mathbf{E}_2 \vec{\sigma}_+ \cdot \mathbf{E}_1^*$ and $\vec{\sigma}_+ \cdot \mathbf{E}_2 \vec{\sigma}_- \cdot \mathbf{E}_1^*$ for linearly cross-polarized pulses, the constant terms in Eqs. (B1) or (B2) become smaller compared with their oscillatory counterparts. Thus the phase changes, until the oscillatory terms become small compared to the constant terms. This occurs on the dephasing time scale.

For strong asymmetry $\kappa_{ee}=0$ and $\kappa_{eh}=2$ we have five bound biexcitons (see the inset of Fig. 7). As shown in Ref. 11, these levels have two-exciton binding energies of 34.7 (the lowest symmetric level), 9.3 (the lowest antisymmetric level), and 0.8 meV (the second lowest symmetric level). The signal has stronger oscillations in Figs. 7–9 compared with Figs. 4–6. This shows that the change of the asymmetry of the Coulomb interaction affects the FWM signal drasti-

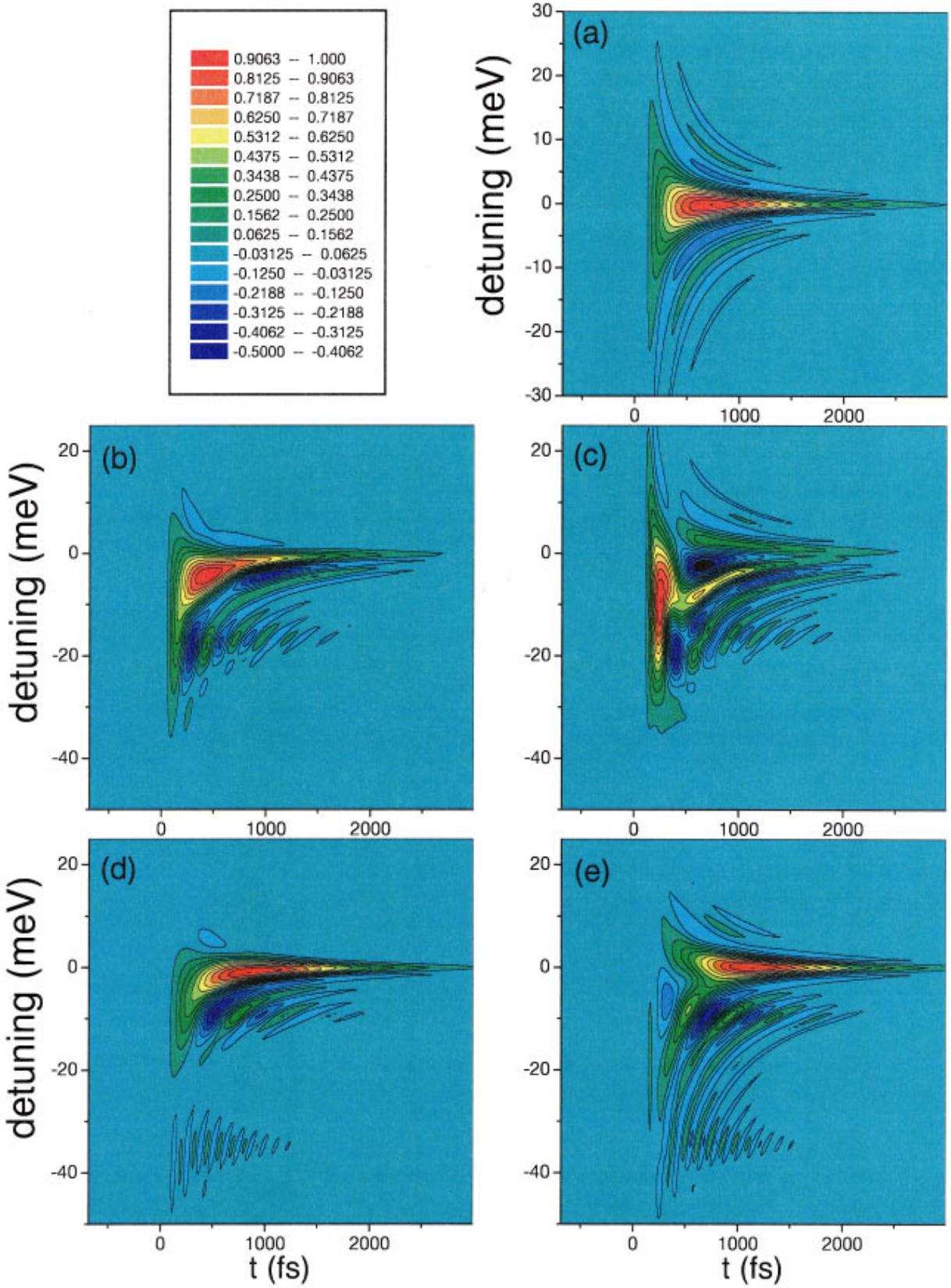


FIG. 11. (Color) Normalized Wigner spectrograms for $T=80$ fs [(a), (c), and (e)], and $T=-80$ fs [(b) and (d)]. (a) corresponds to $\kappa_{ee}=0$ and $\kappa_{eh}=0$, (b) and (c) correspond to $\kappa_{ee}=0$ and $\kappa_{eh}=1$, and (d) and (e) correspond to $\kappa_{ee}=0$ and $\kappa_{eh}=2$. The detuning is defined with respect to the single-exciton resonance. The color code is the same for all plots.

cally, by changing the two-exciton energy levels and their contribution to the FWM signal.

The time-resolved amplitude [(a) and (c)] and phase [(b) and (d)] of the linearly cross-polarized signals are shown in Figs. 10(a) and 10(b) (for $\kappa_{ee}=0$ and $\kappa_{eh}=1$) and Figs. 10(c) and 10(d) (for $\kappa_{ee}=0$ and $\kappa_{eh}=2$). For positive time delays, this technique is known as the photon echo. However, since we only have two degenerate one-exciton states and no inhomogeneous broadening, we do not observe an echo at $t=2T$. Instead, we can see the effect of interference (quantum beats) originating from the energies of the two-exciton states as a function of $t$ for fixed $T$. In the direction $t=T+T_0$ the signal simply decays as $\exp(-\gamma_1 t/\hbar)$.

A different behavior is seen for negative time delays where the Coulomb part of the signal does not only depend on $t-T$ but also on $T$ for the short-pulse limit. This is clearly seen in Fig. 10. Compared with positive time delays, the amplitude changes slowly with $t$, resulting in larger changes of amplitude with $T$. Because of the finite duration of the exciting pulse, the phase of the FWM signal starts to change when $\mathbf{E}_2$ reaches its maximum. The large peak at about $T=-200$ fs in Fig. 10 (a) results from constructive interference of the lowest symmetric and the lowest antisymmetric two-exciton levels. Since the biexciton binding energies are larger for larger asymmetry of the Coulomb interaction, we can see a peak about $T=-150$ fs in Fig. 10(c), i.e., the amplitude for FWM signal for $\kappa_{ee}=0$ and $\kappa_{eh}=2$ reaches its maximum faster than for $\kappa_{ee}=0$ and $\kappa_{eh}=1$. In Fig. 10(c), we observe a weak signal for $T=-400$ fs. This indicates that the signal is dominated by the lowest level of the antisymmetric wave function, which has a two-exciton binding energy 9.3 meV (corresponding to a 450-fs period).

The complex valued time-resolved signal field $S$ may be conveniently displayed using its Wigner spectrogram[62,63] (WS) defined by

$$S_{WS}(t,\omega,T)=\int_{-\infty}^{\infty} S^*\left(t-\frac{t'}{2},T\right)S\left(t+\frac{t'}{2},T\right)e^{i\omega t'}dt'. \tag{3.6}$$

The WS is by definition a real quantity which may have positive and negative values, and depends on the observation time, the frequency, and the time delay. Upon integrating the WS over time (frequency), we obtain the amplitudes of the ordinary frequency-resolved (time-resolved) FWM signals[62]

$$|S(\omega,T)|^2=\int_{-\infty}^{\infty} S_{WS}(t,\omega,T)dt, \tag{3.7}$$

$$|S(t,T)|^2=\int_{-\infty}^{\infty} S_{WS}(t,\omega,T)d\omega. \tag{3.8}$$

The WS can be easily constructed from experiments[15,64,65] in which both the amplitude and the phase of the signal field are measured. It has been used to analyze signatures of correlations in ultrafast FWM on conjugated polyenes[22] and two-exciton states in light-harvesting antenna systems.[66]

In Fig. 11 the WS for our system is displayed for different time delays and asymmetries. Without any asymmetry there are no bound two-exciton states and the contribution to the FWM due to Coulomb scattering vanishes. In this case the time-resolved amplitude shows no beats and the dynamics of the phase is negligible; see Fig. 3. Therefore the magnetoexciton system behaves as an effective two-level system[11] (due to the finite basis set used in our calculations we still have a small Coulomb contribution; see Fig. 3 and discussion). This is consistent with the WS displayed in Fig. 11(a). The WS is symmetric as a function of the detuning, and for a fixed time $t$ shows modulations as a function of the detuning $\Delta\omega$ which are like $\sin(2\Delta\omega t)/\Delta\omega$.[66] As function of time the WS becomes spectrally narrower, which indicates that for long times the excitation becomes resonant.[22,66] With asymmetry [see Figs. 11(b) and 11(c) for $\kappa_{ee}=0$ and $\kappa_{eh}=1$, and 11(d) and 11(e) for $\kappa_{ee}=0$ and $\kappa_{eh}=2$) bound two-exciton states exist and induce beats in the time-resolved signals and FWM signals for negative delays. The WS's [see Figs. 11(b)–11(e)], therefore, become asymmetric with respect to the detuning. New features appear for negative detuning which are directly related to the biexcitonic resonances. For $\kappa_{ee}=0$ and $\kappa_{eh}=1$ ($\kappa_{eh}=2$) the biexcitonic binding energy is 16.5 meV (34.7 meV), and one can clearly identify contributions of these biexcitons to the WS.

## IV. SUMMARY

In this paper we have applied the nonlinear exciton equations to calculate the third-order response of two-dimensional semiconductors in a strong perpendicular magnetic field. Four-wave-mixing signals provide a direct look into the one- and two-magnetoexcitons manifolds. Our calculations used the analytical classification and numerical evaluation of two-exciton states developed in Ref. 11. Two-exciton states with four different angular momentum are considered. A two-exciton state consisting of two electrons and two holes may have the angular momenta $J=2$, with $J_z=2$, $J_z=0$, and $J_z=-2$; and $J=1$, with $J_z=0$,[11] as shown in Fig. 1. The variation of the signals for different polarizations of the exciting fields may be attributed to the different selection rules in each case. The weak FWM signal for linearly cross-polarized pulses is attributed to the cancellation between the signals coming from the two-exciton levels with different angular momenta. The existence of bound biexcitons depends on the asymmetry of Coulomb interaction. Our calculations demonstrate the unique signatures of these states in femtosecond four-wave-mixing spectroscopy.

## ACKNOWLEDGMENTS

We wish to thank D. S. Chemla and V. M. Axt for fruitful discussions. S.M. wishes to acknowledge the support of the Guggenheim Foundation and the Alexander Van Humboldt Foundation and the hospitality of Professor E. Schlag at the University of Munich. The support of the United States Air Force Office of Scientific Research, Grant No. AFOSR-F496620-96-1-0030, and the National Science Foundation Grants No. PHYS94-15583 and No. CHEM98-14061 is gratefully acknowledged.

## APPENDIX A: NEE's WITH ANGULAR MOMENTUM

In this appendix we develop the equations of motion which can be used to calculate the third-order two-pulse FWM signals. The exciting field consists of two pulses:

$$\mathbf{E}(t)=\mathbf{E}_1(t)e^{i\mathbf{k}_1\cdot\mathbf{r}-i\omega_1 t}+\mathbf{E}_1^*(t)e^{-i\mathbf{k}_1\cdot\mathbf{r}+i\omega_1 t}+\mathbf{E}_2(t)e^{i\mathbf{k}_2\cdot\mathbf{r}-i\omega_2 t}+\mathbf{E}_2^*(t)e^{-i\mathbf{k}_2\cdot\mathbf{r}+i\omega_2 t}$$
$$=\mathbf{E}_1^+(t)e^{-i\omega_1 t}+\mathbf{E}_1^-(t)e^{i\omega_1 t}+\mathbf{E}_2^+(t)e^{-i\omega_2 t}+\mathbf{E}_2^-(t)e^{i\omega_2 t}, \tag{A1}$$

where $\mathbf{E}_{1,2}(t)$ are the pulse envelopes. $\mathbf{E}_i^+$ ($\mathbf{E}_i^-$) ($i=1$, and 2) refer to the components of $\mathbf{E}$ with direction $+\mathbf{k}_i$ ($-\mathbf{k}_i$). This field will create excitations at different directions $\mathbf{k}_s=m\mathbf{k}_1+n\mathbf{k}_2$, where $m$ and $n$ can be any integers. We label these different directional components by the superscript $^{(m|n)}$.

We start with Eqs. (2.8)–(2.13), use the rotating frame, and apply the rotating wave approximation to calculate the FWM signal up to the third-order response, which yields

$$i\hbar\frac{d\langle B_+\rangle^{(0|1)}}{dt}=(\epsilon_0-\omega_2-i\gamma_1)\langle B_+\rangle^{(0|1)}-\mu\vec{\sigma}_-\cdot\mathbf{E}_2^+(t), \tag{A2}$$

$$i\hbar\frac{d\langle B_+^\dagger\rangle^{(-1|0)}}{dt}=-(\epsilon_0-\omega_1+i\gamma_1)\langle B_+^\dagger\rangle^{(-1|0)}+\mu\vec{\sigma}_+\cdot\mathbf{E}_1^-(t), \tag{A3}$$

$$i\hbar\frac{d\langle B_-\rangle^{(0|1)}}{dt}=(\epsilon_0-\omega_2-i\gamma_1)\langle B_-\rangle^{(0|1)}-\mu\vec{\sigma}_+\cdot\mathbf{E}_2^+(t), \tag{A4}$$

$$i\hbar\frac{d\langle B_-^\dagger\rangle^{(-1|0)}}{dt}=-(\epsilon_0-\omega_1+i\gamma_1)\langle B_-^\dagger\rangle^{(-1|0)}+\mu\vec{\sigma}_-\cdot\mathbf{E}_1^-(t), \tag{A5}$$

$$\langle B_+^\dagger\rangle^{(0|1)}=\langle B_+\rangle^{(-1|0)}=\langle B_-^\dagger\rangle^{(0|1)}=\langle B_-\rangle^{(-1|0)}=0, \tag{A6}$$

$$i\hbar\frac{d\langle BB_i\rangle^{(0|2)}}{dt}=\sum_{i_1}(H_{ii_1}-2\omega_2\delta_{ii_1}-i\gamma_2\delta_{ii_1})\langle BB_{i_1}\rangle^{(0|2)}-4\mu\vec{\sigma}_-\cdot\mathbf{E}_2^+(t)r_i\langle B_+\rangle^{(0|1)}, \tag{A7}$$

$$i\hbar\frac{d\langle BB_j\rangle^{(0|2)}}{dt}=\sum_{j_1}(H_{jj_1}-2\omega_2\delta_{jj_1}-i\gamma_2\delta_{jj_1})\langle BB_{j_1}\rangle^{(0|2)}-\mu\vec{\sigma}_-\cdot\mathbf{E}_2^+(t)r_j\langle B_-\rangle^{(0|1)}-\mu\vec{\sigma}_+\cdot\mathbf{E}_2^+(t)r_j\langle B_+\rangle^{(0|1)}, \tag{A8}$$

$$i\hbar\frac{d\langle BB_k\rangle^{(0|2)}}{dt}=\sum_{k_1}(H_{kk_1}-2\omega_2\delta_{kk_1}-i\gamma_2\delta_{kk_1})\langle BB_{k_1}\rangle^{(0|2)}-4\mu\vec{\sigma}_+\cdot\mathbf{E}_2^+(t)r_k\langle B_-\rangle^{(0|1)}, \tag{A9}$$

$$i\hbar\frac{d\langle BB_l\rangle^{(0|2)}}{dt}=\sum_{l_1}(H_{ll_1}-2\omega_2\delta_{ll_1}-i\gamma_2\delta_{ll_1})\langle BB_{l_1}\rangle^{(0|2)}-\mu\vec{\sigma}_-\cdot\mathbf{E}_2^+(t)r_l\langle B_-\rangle^{(0|1)}-\mu\vec{\sigma}_+\cdot\mathbf{E}_2^+(t)r_l\langle B_+\rangle^{(0|1)}, \tag{A10}$$

$$i\hbar\frac{d\langle B_+\rangle^{(-1|2)}}{dt}=(\epsilon_0+\omega_1-2\omega_2-i\gamma_1)\langle B_+\rangle^{(-1|2)}+\frac{1}{\pi}\mu\vec{\sigma}_-\cdot\mathbf{E}_2^+(t)\langle B_+^\dagger\rangle^{(-1|0)}\langle B_+\rangle^{(0|1)}+\sum_{ni}r_nU_{ni}\langle B_+^\dagger\rangle^{(-1|0)}\langle BB_i\rangle^{(0|2)}$$
$$+\sum_{nj}r_nU_{nj}\langle B_-^\dagger\rangle^{(-1|0)}\langle BB_j\rangle^{(0|2)}+\sum_{nl}r_nU_{nl}\langle B_-^\dagger\rangle^{(-1|0)}\langle BB_l\rangle^{(0|2)}, \tag{A11}$$

$$i\hbar\frac{d\langle B_-\rangle^{(-1|2)}}{dt}=(\epsilon_0+\omega_1-2\omega_2-i\gamma_1)\langle B_-\rangle^{(-1|2)}+\frac{1}{\pi}\mu\vec{\sigma}_+\cdot\mathbf{E}_2^+(t)\langle B_-^\dagger\rangle^{(-1|0)}\langle B_-\rangle^{(0|1)}+\sum_{nj}r_nU_{nj}\langle B_+^\dagger\rangle^{(-1|0)}\langle BB_j\rangle^{(0|2)}$$
$$+\sum_{nk}r_nU_{nk}\langle B_-^\dagger\rangle^{(-1|0)}\langle BB_k\rangle^{(0|2)}+\sum_{nl}r_nU_{nl}\langle B_+^\dagger\rangle^{(-1|0)}\langle BB_l\rangle^{(0|2)}. \tag{A12}$$

We have added phenomenological dephasing rates $\gamma_1$ ($\gamma_2$) for one-exciton (two-exciton) states. The polarization in the $2\mathbf{k_2}-\mathbf{k_1}$ direction is given by

$$P_x^{(-1|2)}=\frac{\mu}{\sqrt{2}}\{B_+^{(-1|2)}+B_-^{(-1|2)}\}, \tag{A13}$$

$$P_y^{(-1|2)}=-\frac{i\mu}{\sqrt{2}}\{B_+^{(-1|2)}-B_-^{(-1|2)}\}. \tag{A14}$$

## APPENDIX B: IMPULSIVE SIGNALS

In this appendix we derive expressions for the signals in the impulsive limit. For short pulses, with a duration much smaller than the time scale of the coherent dynamics, with a time delay $T$, we can set $\mathbf{E}_2^+(t)=\mathbf{E}_2\delta(t-T)$ and $\mathbf{E}_1^-(t)=\mathbf{E}_1^*\delta(t)$, and solve Eqs. (A2)–(A12) as follows

$$\langle B_+\rangle^{(-1|2)}(t,T)=-\frac{i}{\hbar}\frac{\mu\vec{\sigma}_-\cdot\mathbf{E}_2}{\hbar}\exp\left(-i\frac{\epsilon_0+\omega_1-2\omega_2}{\hbar}t-\frac{\gamma_1}{\hbar}t\right)\left\{\frac{1}{2\pi}\theta(T)\,\theta(t-T)\frac{\mu\vec{\sigma}_-\cdot\mathbf{E}_2}{\hbar}\frac{\mu\vec{\sigma}_+\cdot\mathbf{E}_1^*}{\hbar}\right.$$
$$\left.\times\exp\left(i\frac{2\epsilon_0+\omega_1-3\omega_2}{\hbar}T\right)+2\frac{\mu\vec{\sigma}_-\cdot\mathbf{E}_2}{\hbar}\frac{\mu\vec{\sigma}_+\cdot\mathbf{E}_1^*}{\hbar}\sum_{i_1}K_{i_1}+\frac{\mu\vec{\sigma}_+\cdot\mathbf{E}_2}{\hbar}\frac{\mu\vec{\sigma}_-\cdot\mathbf{E}_1^*}{\hbar}\left(\sum_{j_1}K_{j_1}+\sum_{l_1}K_{l_1}\right)\right\},\tag{B1}$$

$$\langle B_-\rangle^{(-1|2)}(t,T)=-\frac{i}{\hbar}\frac{\mu\vec{\sigma}_+\cdot\mathbf{E}_2}{\hbar}\exp\left(-i\frac{\epsilon_0+\omega_1-2\omega_2}{\hbar}t-\frac{\gamma_1}{\hbar}t\right)\left\{\frac{1}{2\pi}\theta(T)\,\theta(t-T)\frac{\mu\vec{\sigma}_+\cdot\mathbf{E}_2}{\hbar}\frac{\mu\vec{\sigma}_-\cdot\mathbf{E}_1^*}{\hbar}\right.$$
$$\left.\times\exp\left(i\frac{2\epsilon_0+\omega_1-3\omega_2}{\hbar}T\right)+2\frac{\mu\vec{\sigma}_+\cdot\mathbf{E}_2}{\hbar}\frac{\mu\vec{\sigma}_-\cdot\mathbf{E}_1^*}{\hbar}\sum_{k_1}K_{k_1}+\frac{\mu\vec{\sigma}_-\cdot\mathbf{E}_2}{\hbar}\frac{\mu\vec{\sigma}_+\cdot\mathbf{E}_1^*}{\hbar}\left(\sum_{j_1}K_{j_1}+\sum_{l_1}K_{l_1}\right)\right\}.\tag{B2}$$

The first term in the brackets of Eq. (B1) and (B2) correspond to Pauli blocking (phase-space filling), whereas the terms which contain $K_n(t,T)$ $(n=i,j,k,l)$ are related to the Coulomb-interaction and are given by

$$K_n(t,T)=\frac{\hbar f_n}{\omega_1-\omega_2+\Delta_n+i\gamma_2}\exp\left(i\frac{2\epsilon_0-\Delta_n-2\omega_2}{\hbar}T+\frac{\gamma_2}{\hbar}T\right)\left\{\theta(t)\,\theta(-T)\left[\exp\left(i\frac{\omega_1-\omega_2+\Delta_n}{\hbar}t-\frac{\gamma_2}{\hbar}t\right)-1\right]+\theta(t-T)\,\theta(T)\right.$$
$$\left.\times\left[\exp\left(i\frac{\omega_1-\omega_2+\Delta_n}{\hbar}t-\frac{\gamma_2}{\hbar}t\right)-\exp\left(i\frac{\omega_1-\omega_2+\Delta_n}{\hbar}T-\frac{\gamma_2}{\hbar}T\right)\right]\right\}.\tag{B3}$$

Here $\Delta_n$ are the two-exciton Hamiltonian eigenvalues[11] as follows:

$$(2\epsilon_0-\Delta_n)\,\delta_{n,n'}=\sum_{n_1n_2}(S^t)_{nn_1}H_{n_1n_2}S_{n_2n'},\tag{B4}$$

where $S$ is the orthonormal matrix which diagonalizes the two-exciton Hamiltonian. $f_n$ is defined by

$$f_n=\sum_{n_1n_2n_3}r_{n_1}U_{n_1n_2}S_{n_2n}(S^t)_{nn_3}r_{n_3}.\tag{B5}$$

We next consider the relative phase of the Coulomb interaction term for some limiting cases. For $T=0$ and for the small positive time $t$, the Coulomb interaction part of $\langle B_+\rangle^{(-1|2)}$ may be approximated by the short-time expansion

$$\langle B_+\rangle^{(-1|2)}_{Coulomb}(0,t)\sim\left(2\frac{\mu\vec{\sigma}_-\cdot\mathbf{E}_2}{\hbar}\frac{\mu\vec{\sigma}_+\cdot\mathbf{E}_1^*}{\hbar}\sum_{i_1}f_{i_1}+\frac{\mu\vec{\sigma}_+\cdot\mathbf{E}_2}{\hbar}\frac{\mu\vec{\sigma}_-\cdot\mathbf{E}_1^*}{\hbar}\left(\sum_{j_1}f_{j_1}+\sum_{l_1}f_{l_1}\right)\right]\frac{\mu\vec{\sigma}_-\cdot\mathbf{E}_2}{\hbar^2}$$
$$\times\left(t-i\frac{\epsilon_0+\omega_1/2-3\omega_2/2-i\gamma_1-i\gamma_2/2}{\hbar}t^2\right)+i\left[2\frac{\mu\vec{\sigma}_-\cdot\mathbf{E}_2}{\hbar}\frac{\mu\vec{\sigma}_+\cdot\mathbf{E}_1^*}{\hbar}\right.$$
$$\left.\times\sum_{i_1}f_{i_1}\frac{\Delta_{i_1}}{\hbar}+\frac{\mu\vec{\sigma}_+\cdot\mathbf{E}_2}{\hbar}\frac{\mu\vec{\sigma}_-\cdot\mathbf{E}_1^*}{\hbar}\left(\sum_{j_1}f_{j_1}\frac{\Delta_{j_1}}{\hbar}+\sum_{l_1}f_{l_1}\frac{\Delta_{l_1}}{\hbar}\right)\right]\frac{\mu\vec{\sigma}_-\cdot\mathbf{E}_2}{2\hbar^2}t^2.\tag{B6}$$

Since $f_n$ is real, the phase of $\langle B_+\rangle^{(-1|2)}$ is determined by $\vec{\sigma}_+\cdot\mathbf{E}_2$ and $\vec{\sigma}_-\cdot\mathbf{E}_1^*$. We need to consider the second-order term in $t$ when the coefficient of the first-order term is almost zero. For $T=0$ and for large $t$ with $\epsilon_0=\omega_1=\omega_2$, we have

$$\langle B_+\rangle^{(-1|2)}_{Coulomb}(0,t)\sim i\frac{\mu\vec{\sigma}_-\cdot\mathbf{E}_2}{\hbar}\exp\left(-\frac{\gamma_1}{\hbar}t\right)\left[2\frac{\mu\vec{\sigma}_-\cdot\mathbf{E}_2}{\hbar}\frac{\mu\vec{\sigma}_+\cdot\mathbf{E}_1^*}{\hbar}\sum_{i_1}\frac{f_{i_1}}{\Delta_{i_1}+i\gamma_2}+\frac{\mu\vec{\sigma}_+\cdot\mathbf{E}_2}{\hbar}\frac{\mu\vec{\sigma}_-\cdot\mathbf{E}_1^*}{\hbar}\right.$$
$$\left.\times\left(\sum_{j_1}\frac{f_{j_1}}{\Delta_{j_1}+i\gamma_2}+\sum_{l_1}\frac{f_{l_1}}{\Delta_{l_1}+i\gamma_2}\right)\right].\tag{B7}$$

Thus the phase assumes a limiting value for large times $t$. If $f_n=0$ except for $\Delta_n=0$, we have the same phase in Eqs. (B6) and (B7). For $\Delta_n\neq 0$ with $f_n\neq 0$, there is a phase difference between Eqs. (B6) and (B7). The phase change reflects the contribution to the optical response from two-exciton levels which have an energy difference $\Delta_n$ with respect to twice the one-exciton energy.

*Present address: Department of Chemistry, The University of Hong Kong, Hong Kong. Electronic address: yokojima@yangtze.hku.hk

†Present address: Department of Physics and Material Sciences Center, Philipps University, Renthof 5, D-35032 Marburg, Germany. Electronic address: torsten.meier@physik.uni-marburg.de

[1] M. Jiang, H. Wang, R. Merlin, D. G. Steel, and D. Cardona, Phys. Rev. B **48**, 15 476 (1993).

[2] U. Siegner, M.-A. Mycek, S. Glutsch, and D. S. Chemla, Phys. Rev. Lett. **74**, 470 (1995).

[3] U. Siegner, M.-A. Mycek, S. Glutsch, and D. S. Chemla, Phys. Rev. B **51**, 4953 (1995).

[4] P. Kner, S. Bar-Ad, M. V. Marquezini, D. S. Chemla, and W. Schäfer, Phys. Rev. Lett. **78**, 1319 (1997); P. Kner, W. Schäfer, R. Lövenich, and D. S. Chemla, Phys. Rev. Lett **81**, 5386 (1998).

[5] J. B. Stark, W. H. Knox, D. S. Chemla, W. Schäfer, S. Schmitt-Rink, and C. Stafford, Phys. Rev. Lett. **65**, 3033 (1990).

[6] T. Rappen, J. Schröder, A. Leisse, M. Wegener, W. Schäfer, N. J. Sauer, and T. Y. Chang, Phys. Rev. B **44**, 13 093 (1991).

[7] S. T. Cundiff, M. Koch, W. H. Knox, J. Shah, and W. Stolz, Phys. Rev. Lett. **77**, 1107 (1996).

[8] S.-R. Eric Yang and L. J. Sham, Phys. Rev. Lett. **58**, 2598 (1987).

[9] C. Stafford, S. Schmitt-Rink, and W. Schäfer, Phys. Rev. B **41**, 10 000 (1990).

[10] S. Glutsch and D. S. Chemla, Phys. Rev. B **52**, 8317 (1995).

[11] V. Chernyak, S. Yokojima, T. Meier, and S. Mukamel, Phys. Rev. B **58**, 4496 (1998).

[12] V. Chernyak and S. Mukamel, J. Opt. Soc. Am. B **13**, 1302 (1996).

[13] M. Wegener, D. S. Chemla, S. Schmitt-Rink, and W. Schäfer, Phys. Rev. A **42**, 5675 (1990).

[14] J. Knoester and S. Mukamel, Phys. Rep. **205**, 1 (1991).

[15] D. S. Chemla, J.-Y. Bigot, M.-A. Mycek, S. Weiss, and W. Schäfer, Phys. Rev. B **50**, 8439 (1994).

[16] W. Schäfer, D. S. Kim, J. Shah, T. C. Damen, J. E. Cunningham, K. W. Goossen, L. N. Pfeiffer, and K. Köhler, Phys. Rev. B **53**, 16 429 (1996).

[17] S. Mukamel, *Principles of Nonlinear Optical Spectroscopy* (Oxford University Press, New York, 1995).

[18] H. Haug and S. W. Koch, *Quantum Theory of the Optical and Electronic Properties of Semiconductors*, 3rd ed. (World Scientific, Singapore, 1994).

[19] *Confined Excitations in Molecular and Semiconductor Nanostructures*, edited by S. Mukamel and D. S. Chemla, special issue of Chem. Phys. **210** (1996), pp. 1–388.

[20] Yu. A. Bychkov and É. I. Rashba, Zh. Éksp. Teor. Fiz. **85**, 1826 (1983) [Sov. Phys. JETP **58**, 1062 (1983)].

[21] P. Ring and P. Schuck, *The Nuclear Many-Body Problem* (Springer, New York, 1980).

[22] T. Meier and S. Mukamel, Phys. Rev. Lett. **77**, 3471 (1996).

[23] T. Meier, S. Tretiak, V. Chernyak, and S. Mukamel, Phys. Rev. B **55**, 4960 (1997).

[24] S. Mukamel, Z. Deng, and J. Grad, J. Opt. Soc. Am. B **5**, 804 (1988); J. Knoester and S. Mukamel, Phys. Rev. A **39**, 1899 (1989).

[25] S. Schmitt-Rink, S. Mukamel, K. Leo, J. Shah, and D. S. Chemla, Phys. Rev. A **44**, 2124 (1991).

[26] F. C. Spano and S. Mukamel, Phys. Rev. A **40**, 5783 (1989); Phys. Rev. Lett. **66**, 1197 (1991); J. Chem. Phys. **95**, 7526 (1991).

[27] V. Chernyak and S. Mukamel, Phys. Rev. B **48**, 2470 (1993); J. Chem. Phys. **100**, 2953 (1994).

[28] J. A. Leegwater and S. Mukamel, Phys. Rev. A **46**, 452 (1992).

[29] O. Dubovsky and S. Mukamel, J. Chem. Phys. **95**, 7828 (1991).

[30] W. Huhn and A. Stahl, Phys. Status Solidi B **124**, 167 (1984).

[31] S. Schmitt-Rink, D. S. Chemla, and H. Haug, Phys. Rev. B **37**, 941 (1988).

[32] M. Lindberg and S. W. Koch, Phys. Rev. B **38**, 3342 (1988).

[33] V. Chernyak, N. Wang, and S. Mukamel, Phys. Rep. **263**, 213 (1995).

[34] T. Meier, V. Chernyak, and S. Mukamel, J. Phys. Chem. B **101**, 7332 (1997).

[35] V. Chernyak and S. Mukamel, Phys. Rev. Lett. **74**, 4895 (1995).

[36] V. Chernyak and S. Mukamel, Phys. Status Solidi **189**, 67 (1995).

[37] O. Kühn, V. Chernyak, and S. Mukamel, J. Chem. Phys. **105**, 8586 (1996).

[38] V. M. Axt and S. Mukamel, Rev. Mod. Phys. **70**, 145 (1998).

[39] V. Chernyak, W. M. Zhang, and S. Mukamel, J. Chem. Phys. **109**, 9587 (1998).

[40] M. Lindberg, Y. Z. Hu, R. Binder, and S. W. Koch, Phys. Rev. B **50**, 18 060 (1994).

[41] G. Bartels, V. M. Axt, K. Victor, A. Stahl, P. Leisching, and K. Köhler, Phys. Rev. B **51**, 11 217 (1995).

[42] V. M. Axt and A. Stahl, Z. Phys. B **93**, 195 (1994); **93**, 205 (1994); K. Victor, V. M. Axt, and A. Stahl, Phys. Rev. B **51**, 14 164 (1995).

[43] Th. Östreich, K. Schönhammer, and L. J. Sham, Phys. Rev. Lett. **74**, 4698 (1995).

[44] V. M. Axt, A. Stahl, E. J. Mayer, P. Haring Bolivar, S. Nüsse, K. Ploog, and K. Köhler, Phys. Status Solidi B **188**, 447 (1995).

[45] V. M. Axt, K. Victor, and T. Kuhn, Phys. Status Solidi B **206**, 189 (1998).

[46] V. M. Axt, K. Victor, and A. Stahl, Phys. Rev. B **53**, 7244 (1996).

[47] G. Bartels, G. C. Cho, T. Dekorsy, H. Kurz, A. Stahl, and K. Köhler, Phys. Rev. B **55**, 16 404 (1997).

[48] H. Wang, K. B. Ferrio, D. G. Steel, Y. Z. Hu, R. Binder, and S. W. Koch, Phys. Rev. Lett. **71**, 1261 (1993).

[49] H. Wang, K. B. Ferrio, D. G. Steel, P. R. Berman, Y. Z. Hu, R. Binder, and S. W. Koch, Phys. Rev. A **49**, 1551 (1994).

[50] Y. Z. Hu, R. Binder, S. W. Koch, S. T. Cundiff, H. Wang, and D. G. Steel, Phys. Rev. B **49**, 14 382 (1994).

[51] T. Rappen, U. G. Peter, M. Wegener, and W. Schäfer, Phys. Rev. B **49**, 10 774 (1994).

[52] B. F. Feuerbacher, J. Kuhl, and K. Ploog, Phys. Rev. B **43**, 2439 (1991).

[53] S. Bar-Ad and I. Bar-Joseph, Phys. Rev. Lett. **68**, 349 (1992).

[54] D. J. Lovering, R. T. Phillips, G. J. Denton, and G. W. Smith, Phys. Rev. Lett. **68**, 1880 (1992).

[55] K. Bott, O. Heller, D. Bennhardt, S. T. Cundiff, P. Thomas, E. J.

Mayer, G. O. Smith, R. Eccleston, J. Kuhl, and K. Ploog, Phys. Rev. B **48**, 17 418 (1993).

[56] K.-H. Pantke, D. Oberhauser, V. G. Lyssenko, J. M. Hvam, and G. Weimann, Phys. Rev. B **47**, 2413 (1993).

[57] E. J. Mayer, G. O. Smith, V. Heuckeroth, J. Kuhl, K. Bott, A. Schulze, T. Meier, D. Bennhardt, S. W. Koch, P. Thomas, R. Hey, and K. Ploog, Phys. Rev. B **50**, 14 730 (1994).

[58] E. J. Mayer, G. O. Smith, V. Heuckeroth, J. Kuhl, K. Bott, A. Schulze, T. Meier, S. W. Koch, P. Thomas, R. Hey, and K. Ploog, Phys. Rev. B **51**, 10 909 (1995).

[59] T. F. Albrecht, K. Bott, T. Meier, A. Schulze, M. Koch, S. T. Cundiff, J. Feldmann, W. Stolz, P. Thomas, Phys. Rev. B **54**, 4436 (1996).

[60] J. A. Leegwater and S. Mukamel, J. Chem. Phys. **101**, 7388 (1994).

[61] K. Bott, E. J. Mayer, G. O. Smith, V. Heuckeroth, M. Hübner, J. Kuhl, T. Meier, A. Schulze, M. Lindberg, S. W. Koch, and P. Thomas, J. Opt. Soc. Am. B **13**, 1026 (1996).

[62] L. Cohen, Proc. IEEE **77**, 941 (1989)

[63] S. Mukamel, J. Chem. Phys. **107**, 4165 (1997).

[64] J.-Y. Bigot, M.-A. Mycek, S. Weiss, R. G. Ulbrich, and D. S. Chemla, Phys. Rev. Lett. **70**, 3307 (1993).

[65] L. Lepetit, G. Cheriaux, and M. Joffre, J. Opt. Soc. Am. B **12**, 2467 (1995); L. Lepetit and M. Joffre, Opt. Lett. **21**, 564 (1996); J.-P. Likforman, M. Joffre, and V. Thierry-Mieg, *ibid.* **22**, 1104 (1997).

[66] T. Meier, V. Chernyak, and S. Mukamel, J. Chem. Phys. **107**, 8759 (1997).